SINTECHCOM: Science, Technology and Communication Journal
Vol. 7, No. 1, October 2026, pp. 217-224, DOI: 10.59190/stc.v7i1.383

# Apodization profiles of fiber Bragg grating spectra in temperature sensor applications

**Septia Putri Ayu[1,*], Saktioto Saktioto[1], Rakhmawati Farma[1], Rahmondia Nanda Setiadi[1], Haryana Mohd Hairi[2]**
[1]Department of Physics, Universitas Riau, Pekanbaru 28293, Indonesia
[2]Department of Physics, Universiti Teknologi MARA, Shah Alam 40450, Malaysia

**ABSTRACT**

The presence of side lobes in the fiber Bragg grating (FBG) reflection spectrum is a critical challenge that can reduce measurement accuracy in optical sensor applications, necessitating a systematic evaluation of apodization techniques as a mitigation strategy. This study investigated the comparative effects of three apodization profiles, namely uniform, Gaussian, and tan hyperbolic, on the spectral characteristics and performance of an sensors-based temperature sensor with a grating length of 10 mm, grating period of 0.535 μm, modulation index of 0.0001, and operating wavelength of 1550 nm, over a temperature range of 20°C to 100°C. The results showed that all three profiles produced an identical thermal sensitivity of 13.725 pm/°C with a deviation of 3.23% from the theoretical value of 14.183 pm/°C. The Gaussian profile demonstrated the most superior side lobe suppression with an average side lobe level (SLL) of -45.51 dB, exceeding the minimum standard of -20 dB by more than 25 dB, far surpassing the uniform (-16.90 dB) and tanh (-18.17 dB) profiles. These findings establish the Gaussian apodization profile as the most optimal configuration, delivering the highest spectral quality without compromising thermal sensitivity.

**ARTICLE INFO**

**Article history:**

Received Jun 10, 2026
Revised Sep 27, 2026
Accepted Oct 11, 2026
Published Oct 31, 2026

**Keywords:**

Apodization
Fiber Bragg Grating
Side Lobe
Simulation
Temperature Sensor

**Copyright (c) 2026:**

Septia Putri Ayu, Saktioto Saktioto, Rakhmawati Farma, Rahmondia Nanda Setiadi

**License:**

This work is licensed under a Creative Commons Attribution 4.0 International License (CC BY).

*Corresponding Author
E-mail address: septia.putri0189@student.unri.ac.id

## 1. INTRODUCTION

The development of fiber optic sensor technology over the past two decades has opened considerable opportunities for accurate and reliable measurement of various physical quantities in complex industrial environments. Among the various types of fiber optic sensors available, fiber Bragg grating (FBG) holds the most widely developed position due to its ability to directly relate changes in physical quantities to measurable Bragg wavelength shifts with high precision [1]. Sensor offers notable advantages including high sensitivity, compact size, immunity to electromagnetic interference, and multiplexing capability that enables the integration of multiple sensing points within a single optical fiber [2].

Fundamentally, this sensor operates based on the Bragg resonance condition, which produces selective reflection at a wavelength of $\lambda_B = 2n_{eff}\Lambda$, where temperature changes induce wavelength shifts through two mechanisms: the thermo-optic effect and thermal expansion of the grating material [3]. When temperature changes, both quantities are simultaneously affected through the thermo-optic effect that alters $n_{eff}$ (expressed by the thermo-optic coefficient $\xi$) and the thermal expansion effect that alters $\Lambda$ (expressed by the thermal expansion coefficient $\alpha$). he Bragg wavelength shift due to temperature change is expressed as shown in Equation (1) [1,4]:

$$\Delta\lambda_B = \Delta T(\xi + \alpha)\lambda_B \quad (1)$$

For silica fiber at a wavelength of 1550 nm, the values $\alpha \approx 0.55 \times 10^{-6}$/°C and $\xi \approx 8.6 \times 10^{-6}$/°C yield a theoretical sensitivity of approximately 14 pm/°C [4]. The sensor temperature sensitivity ($S_T$) s calculated from the linear regression gradient of $\Delta\lambda_B$ against $\Delta T$, such that its theoretical value can be expressed as shown in Equation (2):

$$S_T = \lambda_B(\alpha + \xi) \quad (2)$$

The primary challenge in sensor implementation is the presence of side lobes in the reflection spectrum. Side lobes arise as a consequence of the uniform refractive index modulation distribution that terminates abruptly at both ends of the grating [1]. In wavelength division multiplexing (WDM)-based multiplexing sensor systems where multiple FBGs operate simultaneously within a single optical fiber, side lobes can cause inter-sensor interference and degrade measurement accuracy [5].

The three apodization profiles analyzed in this study have distinct mathematical formulations. The uniform profile is expressed as A(x) = 1 for $0 \le x \le L$, representing a uniform distribution with no variation at the grating ends. The Gaussian profile uses the function $A(x) = \exp[-\ln 2 \times ((x - L/2) / (0.5l))^2]$ for $0 \le x \le L$, producing a bell-shaped curve with smooth transitions. The tan Hyperbolic profile is expressed as $A(x) = 1 + \tanh[1 - 2(x/l)]$ for $L/2 \le x \le L$, providing a steeper transition than Gaussian but smoother than Uniform [3,6]. Although FBG apodization studies have been widely reported in the context of dispersion compensation and WDM systems [7,8], researchers that specifically compares these three primary profiles in the context of temperature sensing with comprehensive quantitative analysis remains limited. This study aims to fill that gap through a systematic comparative analysis using integrated simulations in OptiGrating v4.2 and OptiSystem v11.1.0.53 over a temperature range of 20°C to 100°C.

The spectral characteristics of the Fiber Bragg Grating reflection spectrum relevant to sensor performance evaluation encompass three primary parameters. Peak reflectivity is expressed in decibels (dB) and determines the signal strength available to the detection system. Full width at half maximum (FWHM) is the spectral width at half the peak reflectivity value; based on the transfer matrix method (TMM), this value is inversely proportional to the grating length, such that a longer grating produces a narrower FWHM and better spectral resolution [1]. The side lobe level (SLL) is measured as the ratio of the highest secondary peak to the main peak in dB, with a minimum value of -20 dB serving as the standard for precision sensor applications [9].

## 2. RESEARCH METHODS

This study employed a numerical simulation method using the TMM approach, implemented through two integrated software tools: OptiGrating v4.2 for FBG spectral characterization at the grating level, and OptiSystem v11.1.0.53 for sensor performance verification at the system level. The simulation approach was selected because it enables systematic and controlled parameter exploration without the constraints of physical fabrication, which is appropriate for a comparative study of apodization profiles at this research scale. The research scope was defined by three apodization profiles (uniform, Gaussian, and tanhyperbolic), a temperature range of 20°C to 100°C with 20°C intervals, standard single-mode silica fiber material, and a fixed operating wavelength of 1550 nm.

The grating sensor parameters used in the simulation were designed with reference to a standard single-mode optical fiber configuration with the following specifications: core diameter of 4.15 μm, cladding diameter of 125 μm, core refractive index of 1.4467, cladding refractive index of 1.444, Bragg

wavelength of 1550 nm, grating length of 10 mm, grating period of 0.535 μm, modulation index of 0.0001, and sinusoidal grating shape. These parameters were applied identically across all three apodization profiles to ensure that any differences in results were attributable solely to the differences in apodization function and not to variations in grating configuration.

The research was conducted in four main stages. The first stage involved grating sensor design in OptiGrating, where each apodization profile was modeled using the established grating parameters. Temperature variation was applied incrementally from 20°C to 100°C with 20°C intervals, generating five data points per profile and a total of 15 simulation scenarios. For each scenario, the reflection spectrum was analyzed using the FWHM tool available in the software to directly obtain the values of peak reflectivity, FWHM, SLL, and Bragg wavelength position.

The second stage involved sensor system verification in OptiSystem. The grating design completed in the previous stage was exported and integrated into a sensor system circuit consisting of four main components: a CW laser as the light source at a frequency of 193.5 THz and a power of 1 mW, an ideal optical circulator to separate the incident signal from the reflected signal, a grating sensor component as the sensing element within the system, and an optical spectrum analyzer (OSA) to record the reflection spectrum in the wavelength domain. The spectral readings from the OSA served as validation of the results obtained in the first stage.

The third stage involved quantitative data processing. All Bragg wavelength, FWHM, peak reflectivity, and SLL values from the 15 simulation scenarios were compiled and analyzed. Thermal sensitivity was calculated based on the gradient of the Bragg wavelength shift against temperature change, and the results were then compared with theoretical values derived from the thermo-optic and thermal expansion coefficients of silica material as a reference.

The fourth stage involves a comparative analysis of various apodization profiles based on the three parameters obtained: reflectivity, FWHM, and SLL. The evaluation was conducted by comparing the performance of each profile against the minimum SLL standard of -20 dB applicable for precision sensor applications, as well as the linearity consistency of the Bragg wavelength shift against temperature variation. From this overall process, conclusions are drawn regarding the most optimal apodization profile for grating-based temperature sensor applications.

## 3. RESULTS AND DISCUSSIONS

### 3.1. Reflectivity Spectrum of the Three Apodization Profiles

The simulation results showed that all three apodization profiles produced an identical initial Bragg wavelength of 1550.101 nm at 20°C. This value is consistent with the Bragg condition equation $\lambda_B = 2 \times 1.447 \times 0.5364792 = 1550.1$ nm, confirming that the grating parameters used were correctly calibrated. The reflectivity spectrum of each profile across temperature variations is presented in Figure 1, and a summary of the peak reflectivity values is provided in Table 1.

Based on Figure 1 and Table 1, the uniform profile produced the highest peak reflectivity with an average value of -2.067 dB, equivalent to 62.1% on a linear scale. The high reflectivity of the uniform profile is attributed to the absence of modulation index attenuation at the grating ends, allowing the entire grating length to contribute fully to energy coupling [10]. The tanh profile occupied an intermediate position with an average of -2.160 dB (60.8%), as the tanh function only moderately attenuates the modulation at the grating ends without significantly reducing the coupling strength at the central region [11].

The Gaussian profile produced the lowest peak reflectivity with an average of -5.919 dB, equivalent to 25.6% on a linear scale. This reduction is an inherent consequence of the strong apodization process, which significantly suppresses the modulation index amplitude throughout the grating via a bell-shaped function [3,10].

Regarding the FWHM parameter, the uniform and tan hyperbolic profiles produced highly stable values of approximately 2.924 nm throughout the entire temperature range. The Gaussian profile produced a stable FWHM ranging from 2.44 to 2.97 nm at temperatures of 20°C to 60°C, but decreased to 2.274 nm and 1.986 nm at 80°C and 100°C, respectively. This reduction does not reflect an actual change in the optical properties of the grating; rather, it is a technical artifact arising from the Bragg peak shifting toward the upper boundary of the simulation calculation range of 1552 nm, leaving insufficient spectral space for the software to measure the full curve width [12,13].

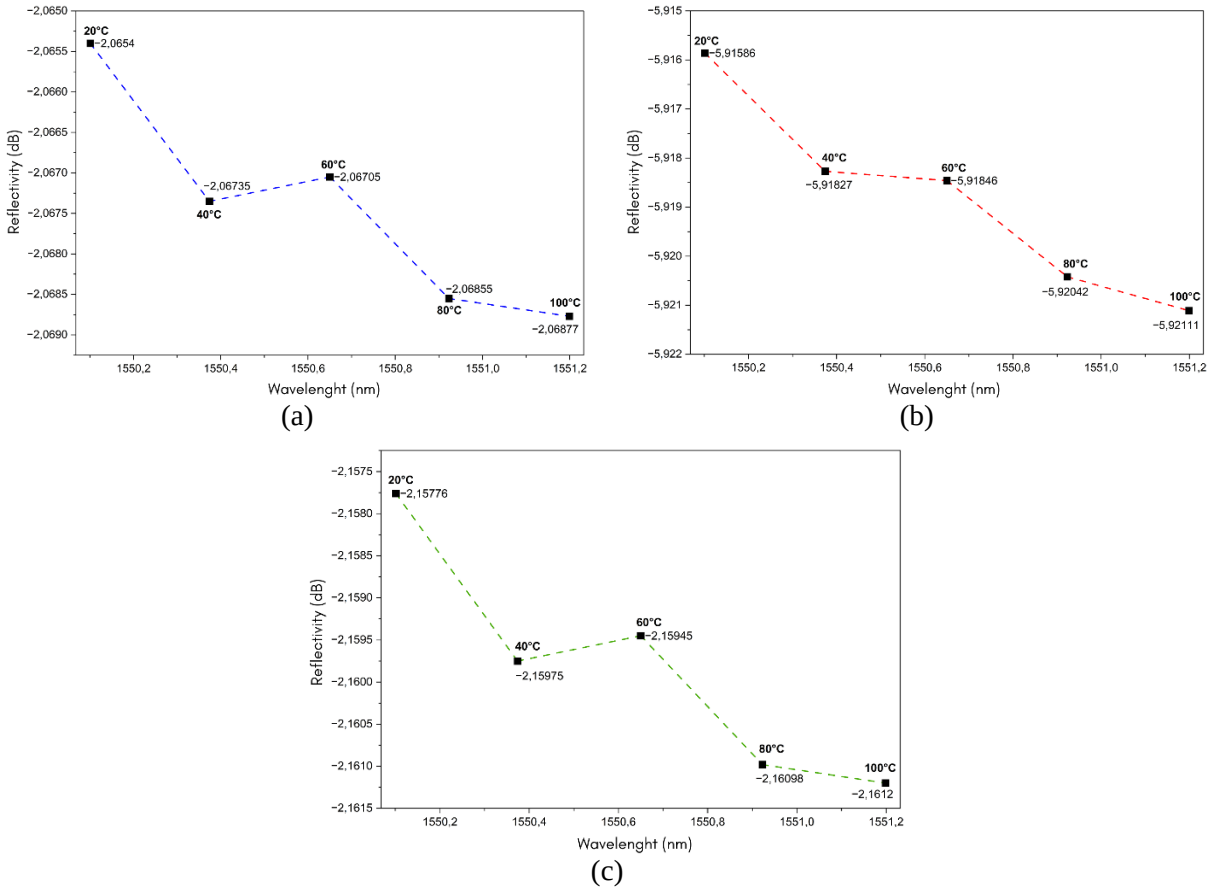



**Figure 1.** Reflectivity spectrum against temperature variation: (a) iniform; (b) Gaussian; and (c) tanh.

**Table 1.** Peak value and peak position of each apodization profile.

| Temperature (°C) | Uniform | | Gaussian | | Tan Hyperbolic | |
|---|---|---|---|---|---|---|
| | Peak position (nm) | Peak value (dB) | Peak Pposition (nm) | Peak value (dB) | Peak position (nm) | Peak value (dB) |
| 20 | 1550.101 | -2.0654 | 1550.101 | -5.91586 | 1550.101 | -2.15776 |
| 40 | 1550.374 | -2.067 | 1550.374 | -5.91827 | 1550.374 | -2.15975 |
| 60 | 1550.650 | -2.067 | 1550.650 | -5.91846 | 1550.650 | -2.15945 |
| 80 | 1550.923 | -2.069 | 1550.923 | -5.92042 | 1550.923 | -2.16098 |
| 100 | 1551.199 | -2.069 | 1551.199 | -5.92111 | 1551.199 | -2.1612 |

The SLL is the most critical parameter distinguishing the performance of the three apodization profiles in this study. SLL-L refers to the left SLL, SLL-R refers to the right SLL, and SLL average is the average of the left and right SLLs [14]. A high SLL can cause ambiguity in reading the Bragg peak position and introduce interference in multiplexed sensor systems, making it the primary determining factor in apodization profile selection for precision sensing applications [3,11]. A comparison of the SLL values across all three profiles is presented in Table 2.

The Uniform profile produced an average SLL of -16.90 dB with a worst-case value of -12.93 dB, which does not meet the minimum standard of -20 dB for precision sensors. The high SLL in the uniform profile is a direct consequence of the uniform refractive index modulation distribution that terminates abruptly at the grating ends, creating strong partial reflections at secondary wavelengths [1,15]. The Gaussian profile demonstrated far superior SLL performance with a consistent value of approximately -45.51 dB throughout the entire temperature range, varying by only ± 0.01 dB. This value exceeds the minimum standard of -20 dB by more than 25 dB [3,16]. On a linear scale, the Gaussian side lobe peak is approximately 35,000 times weaker than its main reflection peak, rendering

interference from side lobes practically negligible in the process of determining the Bragg peak [5]. The Tan Hyperbolic profile produced an average SLL of -18.17 dB with a worst-case value of -13.47 dB, nearly equivalent to the uniform profile under certain conditions. These results indicate that Tanh does not consistently provide meaningful side lobe suppression advantages over uniform for precision sensor applications [13,17].

**Table 2.** SLL values of each apodization profile at each temperature.

| Temperature (°C) | Uniform | | | Gaussian | | Tan Hyperbolic | |
|---|---|---|---|---|---|---|---|
| | SLL-L (dB) | SLL-R (dB) | SLL average (dB) | SLL-L (dB) | SLL-R (dB) | SLL average (dB) | |
| 20 | -17.347 | -17.35 | -17.35 | -45.51 | -45.512 | -45.51 | |
| 40 | -12.931 | -17.35 | -15.14 | -45.52 | -45.522 | -45.52 | |
| 60 | -20.27 | -17.36 | -18.81 | -45.51 | -45.516 | -45.51 | |
| 80 | -12.94 | -20.27 | -16.61 | -45.52 | -45.523 | -45.52 | |
| 100 | -20.27 | -12.94 | -16.61 | -45.52 | -45.52 | -45.51 | |

### 3.2. Bragg Wavelength Shift Response to Temperature Variation

The simulation results showed that all three apodization profiles produced identical and consistent Bragg wavelength shifts at each temperature variation (Table 3). The Bragg wavelength shifted progressively toward longer wavelengths from 1550.101 nm at 20°C to 1551.199 nm at 100°C, with a total shift of 1.098 nm (1098 pm) over a range of $\Delta T$ = 80°C. The linear shift graphs against temperature variation for all three profiles are presented in Figure 2, and the complete data are provided in Table 3.

**Table 3.** Bragg wavelength shift for each apodization profile.

| Temperature (°C) | $\Delta T$ from $T_0$ (°C) | $\lambda_B$ uniform (nm) | $\lambda_B$ Gaussian (nm) | $\lambda_B$ tanh (nm) | $\Delta\lambda_B$ (nm) | $\Delta_\lambda$ per interval (nm) |
|---|---|---|---|---|---|---|
| 20 | 0 | 1550.101 | 1550.101 | 1550.101 | 0 | - |
| 40 | 20 | 1550.374 | 1550.374 | 1550.374 | 0.273 | 0.273 |
| 60 | 40 | 1550.650 | 1550.650 | 1550.650 | 0.549 | 0.276 |
| 80 | 60 | 1550.923 | 1550.923 | 1550.923 | 0.822 | 0.273 |
| 100 | 80 | 1551.199 | 1551.199 | 1551.199 | 1.098 | 0.276 |

Based on Table 3 and Figure 2, all three profiles exhibited identical and consistent Bragg wavelength shifts with increasing temperature. At 20°C, the Bragg wavelength was positioned at 1550.101 nm for all three profiles. As the temperature increased, a progressive shift toward longer wavelengths occurred, reaching 1551.199 nm at 100°C, with a total shift of 1.098 nm over a range of $\Delta T$ = 80°C. The shift per 20°C interval was highly consistent, ranging from 0.273 to 0.276 nm, with a variation of less than 1.1%, confirming excellent linearity of the sensor response [3,18]. The identical shifts observed across all three profiles are fully consistent with theory, as the apodization profile only governs the distribution of the refractive index modulation amplitude without altering the values of $n_{eff}$ or the grating period that determine the Bragg resonance position [1].

### 3.3. Temperature Sensitivity Analysis

Thermal sensitivity was calculated from the linear regression gradient of $\Delta\lambda_B$ against $\Delta T$ for each profile. All three apodization profiles produced an identical sensitivity value of 13.725 pm/°C, with a deviation of only 3.23% from the theoretical value of 14.183 pm/°C. This value closely aligns with previously reported results of 14.00 pm/°C [12], 13.725 pm/°C [11], and 13.71 pm/°C [16] for comparable fiber configurations. The identical sensitivity across all three profiles directly confirms the equation $S_T = \lambda_B(\alpha + \xi)$, which depends solely on the fiber material and operating wavelength, not on the apodization profile applied [1].

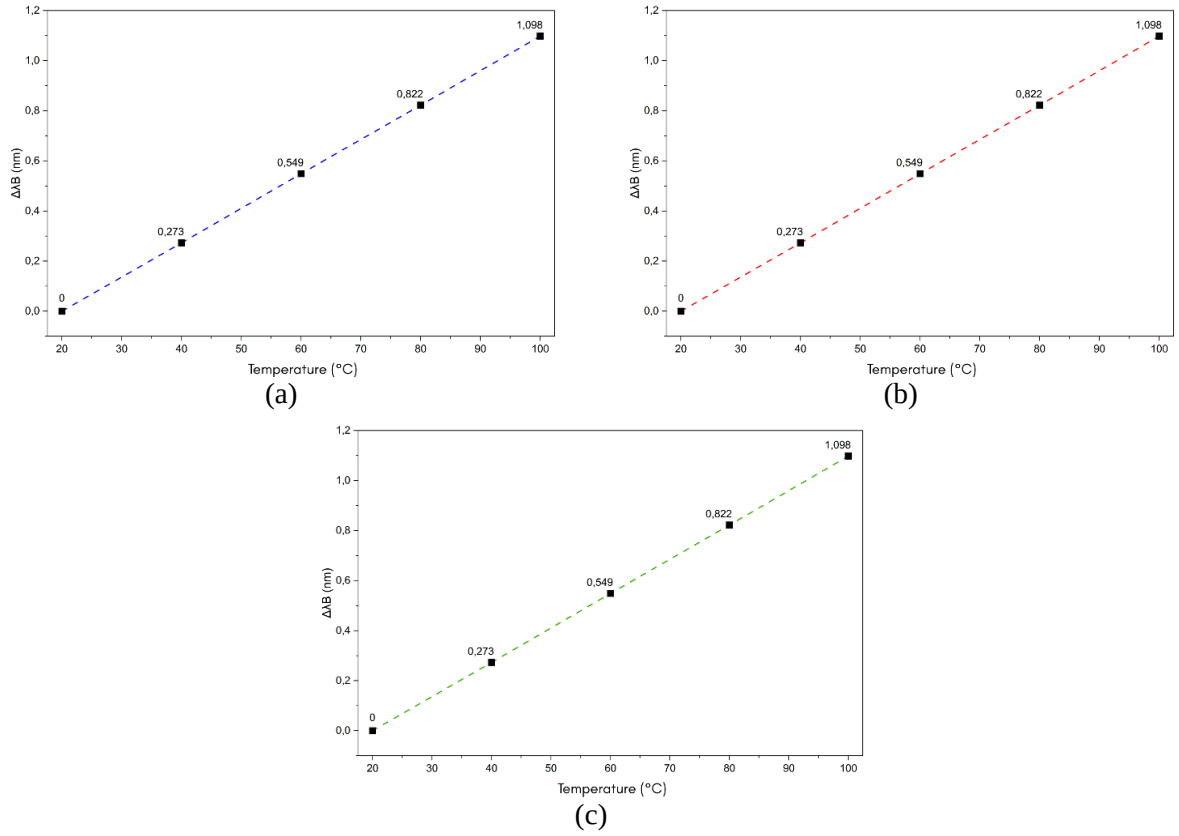



**Figure 2.** Bragg wavelength shift graph against temperature variation: (a) uniform; (b) Gaussian; and (c) tanh.

## 4. CONCLUSION

This of FBGs demonstrated that all three apodization profiles (uniform, Gaussian, and tan hyperbolic) produced an identical thermal sensitivity of 13.725 pm/°C with a deviation of 3.23% from the theoretical value of 14.183 pm/°C. However, the profiles exhibited highly significant differences in reflection spectrum quality. The Gaussian profile was superior, with a consistent SLL of -45.51 dB that exceeded the minimum standard of -20 dB for precision sensors, compared to the uniform (-16.90 dB) and tan hyperbolic (-18.17 dB) profiles, which did not meet that standard. Based on a comprehensive evaluation of reflectivity, FWHM, SLL, and Bragg wavelength shift linearity, the Gaussian profile is recommended as the most optimal apodization profile for FBGs-based temperature sensor applications at 1550 nm with a 10 mm grating configuration.

## AUTHOR CONTRIBUTIONS

Septia Putri Ayu: Investigation, simulation implementation, data curation, formal analysis, visualization, and writing—original draft. Saktioto Saktioto: Conceptualization, methodology, supervision, interpretation of spectral characteristics, and writing—review and editing. Rakhmawati Farma: Methodological refinement, validation, interpretation of temperature-sensing results, and writing—review and editing. Rahmondia Nanda Setiadi: Simulation review, comparative analysis of apodization profiles, verification of sensitivity calculations, and writing—review and editing. Haryana Mohd Hairi: Critical interpretation of findings, assessment of spectral performance, and writing—review and editing. All authors discussed the results, revised the manuscript, and approved the final version.

## FUNDING STATEMENT

This research was funded by DPPM, Kemendiktisaintek, under Main Contract No. 109/C3/DT.05.00/PL-MULTITAHUN LANJUTAN/2026 and Subcontract No. 212/UN19.5.1.3/AL.04/2026, and by Ditjen Risbang, Kemendiktisaintek, in 2026 under Main Contract No. 102/SPK/C.C4/PPK.DHK/IV/2026 and Subcontract No. 283/UN19.5.1.3/AL.04/2026.

## DECLARATION OF AI USE

The authors declare that no AI tools were used in preparing this manuscript.

## CONFLICT OF INTEREST

The authors declare no conflicts of interest.

## DATA AVAILABILITY STATEMENT

All data supporting this study are included in the article. No separate datasets are available.

## ETHICAL APPROVAL

Ethical approval was unnecessary, as no humans or animals were involved.

## ACKNOWLEDGMENTS

The authors gratefully acknowledge Universitas Riau for its institutional support and the Plasma and Photonics Laboratory, Department of Physics, Faculty of Mathematics and Natural Sciences, for providing simulation facilities and computational resources. This research was financially supported by DPPM, Kemendiktisaintek, under Main Contract No. 109/C3/DT.05.00/PL-MULTITAHUN LANJUTAN/2026 and Subcontract No. 212/UN19.5.1.3/AL.04/2026, and by Ditjen Risbang, Kemendiktisaintek, in 2026 under Main Contract No. 102/SPK/C.C4/PPK.DHK/IV/2026 and Subcontract No. 283/UN19.5.1.3/AL.04/2026. Appreciation is also extended to all individuals who contributed through academic discussions and guidance in analysing and interpreting the results.

## REFERENCES

[1] Erdogan, T. (1997). Fiber grating spectra. *Journal of Lightwave Technology*, **15**(8), 1277-1294. DOI: https://doi.org/10.1109/50.618322

[2] Sahota, J. K., Gupta, N., & Dhawan, D. (2020). Fiber Bragg grating sensors for monitoring of physical parameters: A comprehensive review. *Optical engineering*, **59**(6), 060901-060901. DOI: https://doi.org/10.1117/1.OE.59.6.060901

[3] Kersey, A. D., Davis, M. A., Patrick, H. J., LeBlanc, M., Koo, K. P., Askins, C. G., Putnam, M. A., & Friebele, E. J. (1997). Fiber grating sensors. *Journal of Lightwave Technology*, **15**(8), 1442-1463. DOI: https://doi.org/10.1109/50.618377

[4] Othonos, A. (1997). Fiber Bragg gratings. *Review of Scientific Instruments*, **68**(12), 4309-4341. DOI: https://doi.org/10.1063/1.1148392

[5] Qiu, Z., Su, K., Wang, X., & Teng, Y. (2024). Research on sensitized fiber Bragg grating temperature sensor based on bimetal three-substrates. *Review of Scientific Instruments*, **95**(4). DOI: https://doi.org/10.1063/5.0196836

[6] Nsengiyumva, I., Mwangi, E., & Kamucha, G. (2022). Performance analysis of a linear Gaussian- and tanh-apodized FBG and dispersion compensating fiber design for chromatic dispersion compensation in long-haul optical communication networks. *International Journal of Optics*, **2022**, 5734420. DOI: https://doi.org/10.1155/2022/5734420

[7] Mishra, M. & Sahu, P. K. (2022). A study on apodization profiles of fiber Bragg gratings. In M. N. Mohanty & S. Das (Eds.), *Advances in intelligent computing and communication*, 183-189. DOI: https://doi.org/10.1007/978-981-19-0825-5_19

[8] Udd, E., & Spillman, W. B., Jr. (Eds.). (2024). *Fiber optic sensors: An introduction for engineers and scientists* (3rd ed.). John Wiley & Sons. DOI: https://doi.org/10.1002/9781119678892

[9] Bhaskar, C. V. N., Pal, S., & Pattnaik, P. K. (2021). Recent advancements in fiber Bragg gratings based temperature and strain measurement. *Results in Optics*, **5**, 100130. DOI: https://doi.org/10.1016/j.rio.2021.100130

[10] Chaoui, F., Aghzout, O., Chakkour, M., & El Yakhloufi, M. (2016). Apodization optimization of FBG strain sensor for quasi-distributed sensing measurement applications. *Active and Passive Electronic Components*, **2016**, 6523046.
DOI: https://doi.org/10.1155/2016/6523046

[11] Mandal, H. N., & Sidhishwari, S. (2023). Sensitivity analysis of designed apodized fiber Bragg grating sensor using artificial neural network and tree-based models. *Results in Optics*, **10**, 100343.
DOI: https://doi.org/10.1016/j.rio.2022.100343

[12] Tahhan, S. R., Ali, M. H., Al-Ogaidi, M. A. Z., & Abass, A. K. (2019). Impact of apodization profile on performance of fiber Bragg grating strain–temperature sensor. *Journal of Communications*, **14**(1), 53-57.
DOI: https://doi.org/10.12720/jcm.14.1.53-57

[13] Maiti, S., & Singh, V. (2022). Performance analysis of apodized fiber Bragg gratings for sensing applications. *Silicon*, **14**(2), 581-587.
DOI: https://doi.org/10.1007/s12633-020-00852-0

[14] Maulana, A. M., Ramadhan, K., & Irawan, D. (2023). Analysis of fluid flow in a cylindrical tube using fiber Bragg grating. *Science, Technology, and Communication Journal*, **4**(1), 17-22.
DOI: https://doi.org/10.59190/stc.v4i1.253

[15] Irawan, D., Ramadhan, K., Saktioto, & Marwin, A. (2022). Performance comparison of TOPAS chirped fiber Bragg grating sensor with Tanh and Gaussian apodization. *Indonesian Journal of Electrical Engineering and Computer Science*, **26**(3), 1477-1485.
DOI: https://doi.org/10.11591/ijeecs.v26.i3.pp1477-1485

[16] Saktioto, T., Ramadhan, K., Soerbakti, Y., Irawan, D., & Okfalisa. (2021). Integration of chirping and apodization of Topas materials for improving the performance of fiber Bragg grating sensors. *Journal of Physics: Conference Series*, **2049**(1), 012001.
DOI: https://doi.org/10.1088/1742-6596/2049/1/012001

[17] Kumari C.R., U., Samiappan, D., & Sudhakar, T. (2020). Development and experimental validation of a Nuttall apodized fiber Bragg Grating sensor with a hydrophobic polymer coating suitable for monitoring sea surface temperature. *Optical Fiber Technology*, **56**, 102176.
DOI: https://doi.org/10.1016/j.yofte.2020.102176

[18] Ramadhan, K., Irawan, D., & Yupapin, P. (2023). Core multi-layer dispersion on single-mode optical fiber. *Science, Technology, and Communication Journal*, **3**(3), 89-94.
DOI: https://doi.org/10.59190/stc.v3i3.235